Volume 11
Number 21
7 June 2020
Pages 5349–5602

Chemical Science

rsc.li/chemical-science

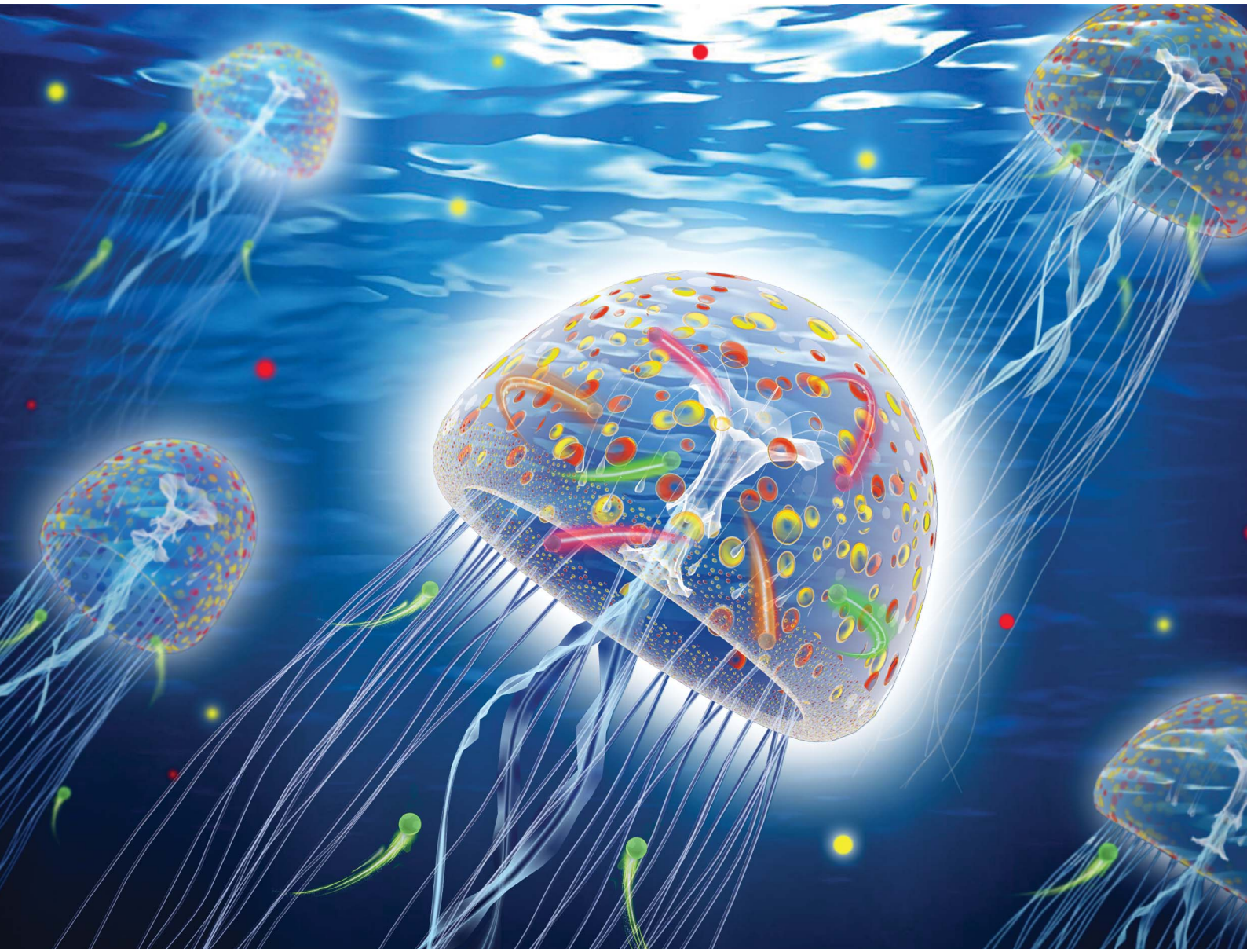

ISSN 2041-6539

ROYAL SOCIETY OF CHEMISTRY

EDGE ARTICLE

Ying Zhuo *et al.*

Covalent organic frameworks as micro-reactors: confinement-enhanced electrochemiluminescence

Chemical Science

ROYAL SOCIETY OF CHEMISTRY

EDGE ARTICLE

Cite this: *Chem. Sci.*, 2020, **11**, 5410

All publication charges for this article have been paid for by the Royal Society of Chemistry

Covalent organic frameworks as micro-reactors: confinement-enhanced electrochemiluminescence†

Wei-Jia Zeng,[ab] Kun Wang,[a] Wen-Bin Liang,[a] Ya-Qin Chai,[a] Ruo Yuan[a] and Ying Zhuo*[a]

Electrochemiluminescence (ECL) micro-reactors with enhanced intensity and extreme stability were first established by the assembly of tris(2,2′-bipyridyl) ruthenium(II) ($Ru(bpy)_3^{2+}$) onto covalent organic frameworks (COFs), in which a type of imine-linked COF (denoted as COF-LZU1) was employed as a model for ECL micro-reactors. Compared with the dominant ECL system of $Ru(bpy)_3^{2+}$/tri-*n*-propylamine (TPrA) (TPrA as a co-reactant), the intensity of the COF-LZU1 micro-reactor-based electrode was significantly increased nearly 5-fold under the same experimental conditions, which is unprecedented in other $Ru(bpy)_3^{2+}$-based ECL systems. This enhancement can be attributed to the large surface area, delimited space, and stable and hydrophobic porous structure of COF-LZU1, which not only enabled a huge amount of $Ru(bpy)_3^{2+}$ to be loaded in/on COF-LZU1, but also enriched a large amount of TPrA from the aqueous solution into its inner hydrophobic cavity due to the lipophilicity of TPrA. More importantly, with its hydrophobic porous nanochannels, COF-LZU1 could act as micro-reactors to provide a delimited reaction micro-environment for the electrochemical oxidation of TPrA and the survival of TPrA$^{\bullet}$, achieving significant confinement-enhanced ECL. To prove this principle, these Ru@COF-LZU1 micro-reactors were developed to prepare an ECL aptasensor for aflatoxin M1 (AFM1) detection with a wide detection range and a low detection limit. Overall, this work is the first report in which ECL micro-reactors are constructed with COFs to enhance the intensity and stability of the $Ru(bpy)_3^{2+}$-based ECL system, and opens a new route to the design of other ECL micro-reactors for bioanalysis applications.

Received 30th March 2020
Accepted 29th April 2020

DOI: 10.1039/d0sc01817a

rsc.li/chemical-science

Introduction

The classical electrochemiluminescence (ECL) system, tris(2,2′-bipyridyl) ruthenium(II)/tri-*n*-propylamine ($Ru(bpy)_3^{2+}$/TPrA), has been extensively studied and successfully used in commercial clinical diagnosis owing to its chemical stability and good biocompatibility.[1,2] With increasing demands for high sensitivity methods for trace detection, improvements in ECL intensity and the stability of $Ru(bpy)_3^{2+}$/TPrA have contributed greatly to strengthen its dominant role of ECL technology in bioanalysis.Conventional methods for intensity amplification include increasing the amount of $Ru(bpy)_3^{2+}$ with the use of various nanomaterials, such as assembling $Ru(bpy)_3^{2+}$ on gold nanoparticles (AuNPs)[3] or doping $Ru(bpy)_3^{2+}$ with silica nanoparticles.[4] However, the involvement of nanomaterials might cause the potential problems of (i) ECL quenching owing to the energy transfer between AuNPs and $Ru(bpy)_3^{2+}$,[5] and (ii) poor ECL efficiency of the internal ECL lumiphore.[6] More importantly, ECL intensity does not always increase linearly with amount of $Ru(bpy)_3^{2+}$; thus only enriching the amount of $Ru(bpy)_3^{2+}$ will lead to bottlenecks in achieving enhanced ECL intensity.[7] Herein, we note that the TPrA radical (TPrA$^{\bullet}$) can also play a crucial role in boosting the ECL emission of $Ru(bpy)_3^{2+}$, since the excited states of $Ru(bpy)_3^{2+}$ are generated through the interaction between the active intermediates of $Ru(bpy)_3^{2+}$ and TPrA$^{\bullet}$.[8,9] However, the oxidation efficiency of TPrA (the production efficiency of TPrA$^{\bullet}$) is relatively low due to the poor solubility of TPrA,[10] while the stability of TPrA$^{\bullet}$ is also easily affected by dissolved oxygen in aqueous solution.[11] Therefore, increasing the amount of TPrA$^{\bullet}$ is a more cost-effective method for enhancing ECL intensity, although few reports to date have focused on the improvement of the oxidation efficiency of TPrA.

Compared with traditional reaction vessels, micro/nanoreactors could provide a confined reaction environment on a nanometre scale, which offers great potential to improve

[a]*Chongqing Engineering Laboratory of Nanomaterials & Sensor Technologies, College of Chemistry and Chemical Engineering, Southwest University, Chongqing 400715, China. E-mail: yingzhuo@swu.edu.cn*

[b]*National Engineering Research Center for Modernization of Traditional Chinese Medicine–Hakka Medical Resources Branch, College of Pharmacy, Gannan Medical University, Ganzhou 341000, China*

† Electronic supplementary information (ESI) available: Experimental section and related experimental data. See DOI: 10.1039/d0sc01817a

the efficiency of chemical transformations by concentrating the catalysts and reactants in confined spaces.[12,13] Consequently, considerable efforts have been put into micro/nanoreactor-based proteolysis,[14] enzyme reactions,[15] bio-molecular detection[16] and catalysis[17] to achieve high efficiency, sensitivity, rapid time response and selectivity. It is well known that ECL is achieved at or near the electrode surface from the excited states of luminophores,[18] which greatly depends on the electrochemical reaction between the active intermediates of luminophores and the highly oxidising or reducing radicals of the co-reactants.[19,20] As a result, the productivity of the co-reactant radicals is one of the critical elements affecting the ECL signal dramatically.[21] Thus, we drew inspiration from micro/nanoreactors to achieve confinement-enhanced ECL for the first time, which is very likely to provide a more beneficial reaction micro-environment and improve ECL efficiency.

As a new class of porous materials, the covalent organic frameworks (COFs) are assembled from building units *via* covalent bonds.[22,23] These materials have been widely applied in catalysis,[24] separations[25] and energy storage, among other applications.[26] Previous studies have indicated that the defined pore micro-environment might make COFs desirable nanomaterials for biosensor construction; however, few examples have been reported to date.[27] Thus, inspired by their regular and predictable two- or three-dimensional pore structure and large surface area,[28] $Ru(bpy)_3^{2+}$ assembled imine-linked COFs (Ru@COF-LZU1) were first developed as ECL micro-reactors (Scheme 1A), demonstrating strong ECL intensity and desirable stability. The mechanism (Scheme 1C) indicates that the Ru@COF-LZU1 micro-reactors could not only improve the oxidation efficiency of TPrA by concentrating the TPrA from solution, but could also provide a relatively independent and confined reaction environment for the electrochemical oxidation of TPrA and the survival of TPrA$^{\bullet}$. This achieves a high reaction efficiency between the TPrA$^{\bullet}$ and the intermediate of $Ru(bpy)_3^{2+}$ to obtain more excited states of $Ru(bpy)_3^{2+}$. Hereafter, the Ru@COF-LZU1 micro-reactors were used to develop an ECL platform for aflatoxin M1 (AFM1). As shown in Scheme 1B, the Ru@COF-LZU1 and Pt concave nanocubes (Pt CNCs) were modified on the electrode successively to achieve an extremely intense ECL response as the initial "signal-on" state. Then, the ferrocene (Fc)-labelled probes were immobilised on the modified interface to obtain the "signal-off" state for the background signal minimisation.[29] Subsequently, the target AFM1 was converted to output DNA based on the DNA walker-based amplification strategy (inset of Scheme 1B). Finally, the ECL signal recovered when the output DNA was incubated with the resultant electrode to remove the Fc-labelled probes. With the strong ECL emission of Ru@COF-LZU1 micro-reactors, the ECL biosensor exhibited high sensitivity and stability for AFM1 detection. Meanwhile, this work also sheds light on a novel platform for the ECL enhancement of $Ru(bpy)_3^{2+}$/TPrA, which has opened new routes to the design of other ECL micro-reactors for bioanalysis applications.

Results and discussion

Scanning electron microscopy (SEM) and transmission electron microscopy (TEM) were employed to characterise the morphology of the nanomaterials in this work. As shown in Fig. 1A, the SEM image of COF-LZU1 exhibited a spherical structure, with a size of 200–400 nm. Furthermore, it can clearly be observed that COF-LZU1 exhibits a layered stacking structure in the TEM image (Fig. 1B). Moreover, the local enlarged TEM image of COF-LZU1 (Fig. 1C) exhibits porous structures, which is consistent with previous reports in the literature.[30] Additionally, the structure of COF-LZU1 was studied by both X-ray diffraction (XRD) analysis and Fourier transform infrared (FI-IR) spectroscopy. As shown in Fig. 1D, the XRD pattern of COF-LZU1 shows characteristic 2θ peaks ranging from 1 to 35°, which is consistent with previous reports.[31] The FI-IR spectrum

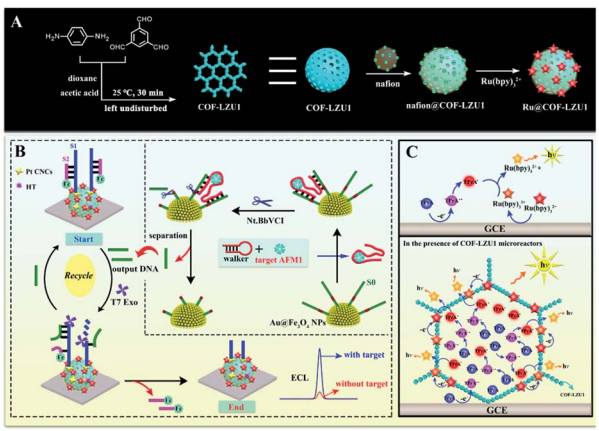

Scheme 1 (A) Preparation of Ru@COF-LZU1 micro-reactors. (B) A schematic illustration of the operating principle of the biosensor for AFM1 determination (the inset shows a schematic illustration of the DNA walker-based amplification strategy). (C) General mechanism of the reaction process between $Ru(bpy)_3^{2+}$ and TPrA (with and without COF-LZU1 micro-reactors).

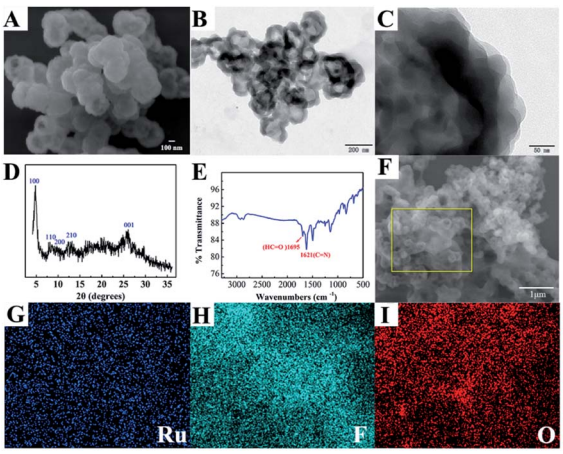

Fig. 1 SEM (A) and TEM images (B) of COF-LZU1. A local enlarged TEM image of COF-LZU1 (C). XRD (D) and FT-IR spectroscopy (E) studies of COF-LZU1. An SEM image of Ru@COF-LZU1 (F), and SEM-EDX elemental mapping analysis of Ru (G), F (H), and O (I) in Ru@COF-LZU1.

is shown in Fig. 1E, and reveals a strong peak at 1621 cm^{-1}, which is attributed to the formation of C=N bonds.

Fig. 1F shows the SEM of Ru@COF-LZU1 entirely entwined by a layer of yarn, which could be the Nafion, as a cross-linker was adsorbed onto the surface of COF-LZU1 according to the electrostatic interaction. Furthermore, energy dispersive spectroscopy (EDS) elemental mapping of Ru (Fig. 1G) and F (Fig. 1H) of Ru@COF-LZU1 were observed, demonstrating the electrostatic adsorption between $Ru(bpy)_3^{2+}$ and Nafion. The element O in COF-LZU1 is also clearly observed in Fig. 1I. The zeta potential values of COF-LZU1, Nafion@COF-LZU1 and Ru@COF-LZU1 were measured at pH = 7.4, respectively, and also confirmed the layer-by-layer assembly of Nafion and $Ru(bpy)_3^{2+}$. The corresponding results are shown in Section 3 of the ESI.†

In order to study the effect of COF-LZU1 micro-reactors on $Ru(bpy)_3^{2+}$/TPrA, the 3D ECL spectrum of the COF-LZU1 modified glassy carbon electrode (GCE) (COF-LZU1/GCE) in test solution containing $Ru(bpy)_3^{2+}$ and TPrA are shown in Fig. 2A with the maximum ECL emission at 630 nm with potential at 1.1 V. A comparison experiment of bare GCE in $Ru(bpy)_3^{2+}$/TPrA (Fig. 2B) was also carried out under the same experimental conditions, which showed the same maximum ECL emission at 630 nm but much weaker ECL intensity than that of COF-LZU1/GCE (Fig. 2A). Fig. 2C shows the ECL-potential profiles of COF-LZU1/GCE (curve *a*) and bare GCE (curve *b*) in $Ru(bpy)_3^{2+}$ + TPrA solution. The ECL signal on COF-LZU1/GCE has increased about 4800 a.u. (curve *a*), a nearly ~5-fold enhancement compared with that of bare GCE (932 a.u). This indicates the significant confinement-enhanced ECL effect on COF-LZU1 micro-reactors.

In order to confirm the confinement effect of COF-LZU1 micro-reactors, cyclic voltammogram (CV) scans on GCE and the COF-LZU1/GCE were measured in TPrA solution, respectively (insert of Fig. 2C). An irreversible anodic peak at 0.84 V was observed when the bare GCE was measured in TPrA solution (curve *c* in insert of Fig. 2C), which is attributed to the electrochemical oxidation of TPrA.[32] As expected, the anodic peak current of curve *d* was increased nearly 3-fold in the presence of COF-LZU1 micro-reactors compared with that of curve *c*, suggesting that the more oxidised state of TPrA was generated in this situation. The reason for this might be that the COF-LZU1 micro-reactors could enrich TPrA in its internal hydrophobic porous structure, resulting in the enhancement of $TPrA^{\bullet}$. Fig. 2D shows the electrochemical oxidation of TPrA with and without COF-LZU1 micro-reactors in the diffusion layer. It can be seen that only a tiny amount of TPrA was electrochemically oxidised in the diffusion layer without the COF-LZU1 in Fig. 2D(a), due to the low solubility of TPrA[10] and the poor stability of $TPrA^{\bullet}$.[11] In contrast, in Fig. 2D(b), a large amount of TPrA was electrochemically oxidised in the diffusion layer in the presence of COF-LZU1 micro-reactors. This is because COF-LZU1 possesses hydrophobic internal porous structures that can serve as micro-reactors, which may not only considerably concentrate TPrA from the solution, but may also provide a more conductive reaction micro-environment for the electrochemical oxidation of TPrA and the survival of $TPrA^{\bullet}$. Therefore, the explanations for the confinement-enhanced ECL with COF-LZU1 micro-reactors could be as follows: (1) as micro-reactors, COF-LZU1 could improve the electrochemical oxidation of TPrA, resulting in the production of more excited states of $Ru(bpy)_3^{2+}$, and (2) the micro-reactors could limit the $Ru(bpy)_3^{2+}$ loaded in/on the COF-LZU1 and the $TPrA^{\bullet}$ in a tiny space, which could substantially improve the ECL efficiency between the $Ru(bpy)_3^{2+}$ and $TPrA^{\bullet}$.

Next, in order to optimise the efficiency and sensitivity of the proposed aptasensor, the cleaving time of Nt. BbvCI restriction endonuclease and the incubation time of T7 Exo were selected as follows. As shown in Fig. 3A, when the cleaving time of Nt. BbvCI restriction endonuclease shifted from 30 to 150 min, the ECL signal increased and the maximum ECL signal was achieved at 120 min. Thus, 120 min was used as the optimal cleavage time. Fig. 3B shows the incubation time of T7 Exo toward the proposed aptasensor. With the increment of the incubation time of T7 Exo, the ECL signal increased rapidly and reached a maximum at 120 min, which was consequently selected as the incubation time of T7 Exo in this work.

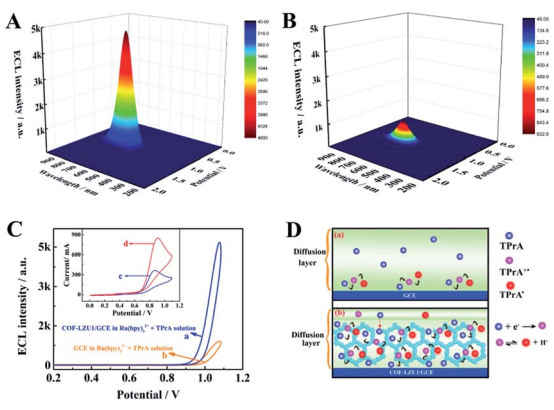

Fig. 2 ECL spectra of COF-LZU1/GCE (A) and a bare GCE (B) test solution containing $Ru(bpy)_3^{2+}$ (0.25 μM) and TPrA (1 mM). (C) ECL-potential profiles of COF-LZU1/GCE in a mixed solution containing $Ru(bpy)_3^{2+}$ (0.25 μM) and TPrA (1 mM) (a), and a GCE in $Ru(bpy)_3^{2+}$ solution (0.25 μM) (b). The inset of (C) shows the CVs of a bare GCE (c) and COF-LZU1/GCE (d) in TPrA solution (5 mM). (D) A schematic illustration of the electrochemical oxidation of TPrA with (a) and without (b) COF-LZU1 in the diffusion layer.

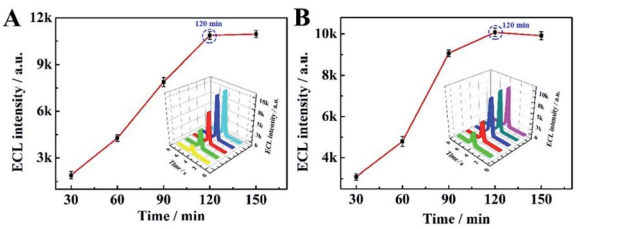

Fig. 3 (A) The influence of Nt. BbvCI restriction endonuclease cleaving time (30 min, 60 min, 90 min, 120 min, 150 min) and (B) the incubation time of T7 Exo (30 min, 60 min, 90 min, 120 min, 150 min) on the ECL response based on the proposed biosensor (AFM1 concentration: 0.3 μg mL^{-1}).

Under the optimum parameter conditions, ECL detection at different concentrations of AFM1 was performed using the proposed method. As shown in Fig. 4, the ECL response increased gradually with AFM1 concentration (Fig. 4A), while the logarithmic value of the response shows a linear dependence on the AFM1 concentration over the range from 0.03 pg mL^{-1} to 0.3 μg mL^{-1} with a correlation coefficient of 0.9982 (Fig. 4B). The linear equation was $I = 1279.62 \lg c + 3624.45$ with a detection limit of 0.009 pg mL^{-1} (the detail calculation was shown in Section 6 of the ESI†). In addition, a comparison of the performance of this aptasensor with that of other reported work (Table S2 in Section 7 of the ESI†), suggests that a wider linear range and a lower detection limit were achieved in this work. Fig. 4C shows the ECL profiles under three cycle potential scans upon the increase of AFM1 concentrations, suggesting the extreme stability of the COF-LZU1 micro-reactor-based biosensor.

To assess the selectivity of the proposed aptasensor, aflatoxinB1 (AFB1), aflatoxinB2 (AFB2), kanamycin, glucose and melamine were selected as interfering substances. It was found the ECL responses exhibited negligible errors when the proposed aptasensors were incubated with AFB1, AFB2, kanamycin, glucose and melamine, respectively, in comparison with that of a blank sample (Fig. 4D). Furthermore, the response of the mixed solution containing the target AFM1 and the above interfering substances was also measured, and the ECL signal was found to be close to that of the AFM1 standard solution. These results indicate that the aptameric recognition function in the proposed aptasensor was adequately retained and with sufficient selectivity for AFM1.

Finally, the feasibility of the proposed aptasensor was assessed by the standard addition/recovery method using defatted milk as real samples. First, the defatted milk was harvested with centrifugation for 20 min at 12 000 rpm using pure milk. Then the AFM1 at different concentrations was added into the defatted samples. As shown in Table 1, the recovery of AFM1 detection is in the range of 93.3–104.0%, demonstrating the potential application of the AFM1 aptasensor in real milk samples.

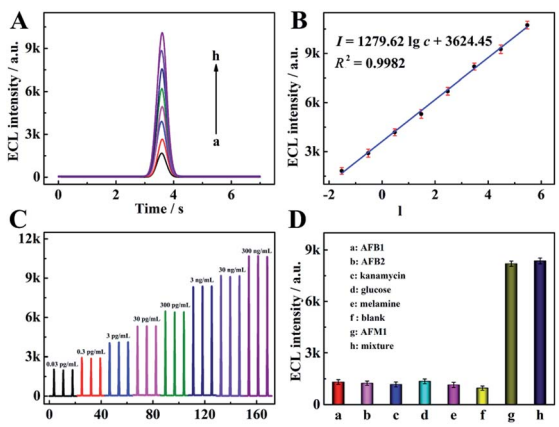

Fig. 4 (A) ECL curve of this proposed aptasensor at different concentrations of AFM1: 0.03 pg mL^{-1}, 0.3 pg mL^{-1}, 3 pg mL^{-1}, 0.03 ng mL^{-1}, 0.3 ng mL^{-1}, 3 ng mL^{-1}, 30 ng mL^{-1}, and 0.3 μg mL^{-1} (from a to h). (B) The corresponding calibration plot of the AFM1 aptasensor. (C) Stability of the proposed aptasensor towards different concentrations of AFM1. (D) Selectivity of the aptasensor towards AFM1 (3 ng mL^{-1}) against interferents: AFB1, AFB2, kanamycin, glucose, melamine, and a mixture (containing the above interferents and 3 ng mL^{-1} AFM1). The concentration of each interferent was 3 μg mL^{-1}.

Table 1 Recovery of AFM1 in defatted milk by the proposed aptasensor

Sample number	Added (ng mL^{-1})	Found (ng mL^{-1})	Recovery (%)
1	0.1	0.104	104.0
2	0.5	0.49	98.0
3	5	5.14	102.8
4	10	9.55	95.5
5	100	93.3	93.3

Conclusions

In summary, a novel Ru@COF-LZU1 micro-reactor-based biosensor was first constructed with confinement-enhanced ECL. Compared with conventional $Ru(bpy)_3^{2+}$-based ECL systems using TPrA as a co-reactant, the COF-LZU1 micro-reactors provided the following significant advantages. First, the COF-LZU1 micro-reactors with hydrophobic porous nanochannels not only improved the oxidation efficiency of TPrA by concentrating TPrA from the solution, but also provided a relatively independent and confined reaction environment for the electrochemical oxidation of TPrA and the survival of $TPrA^{\bullet}$. Second, COF-LZU1 with a large surface area could load large amounts of molecular $Ru(bpy)_3^{2+}$ based on electrostatic interactions. Thus, this work demonstrates confinement-enhanced ECL by COF-LZU1 micro-reactors for the sensitive detection of AFM1, and opens new routes to explore other ECL micro-reactors for bioanalysis applications.

Conflicts of interest

There are no conflicts to declare.

Acknowledgements

This work was financially supported by the NNSF of China (21675130, 21775124, 21974108), the Natural Science Foundation Project of CQ CSTC (cstc2018jcyjAX0546) and the Fundamental Research Funds for the Central Universities (XDJK2019TJ002), China.

References

1 J. J. Zhang, R. Jin, D. C. Jiang and H. Y. Chen, *J. Am. Chem. Soc.*, 2019, **141**, 10294–10299.
2 M. M. Chen, W. Zhao, M. J. Zhu, X. L. Li, C. H. Xu, H. Y. Chen and J. J. Xu, *Chem. Sci.*, 2019, **10**, 4141–4147.
3 Y. Z. Wang, C. H. Xu, W. Zhao, Q. Y. Guan, H. Y. Chen and J. J. Xu, *Anal. Chem.*, 2017, **89**, 8050–8056.

4 C. Ma, W. W. Wu, L. L. Li, S. J. Wu, J. R. Zhang, Z. X. Chen and J. J. Zhu, *Chem. Sci.*, 2018, **9**, 6167–6175.
5 G. H. Zhao, Y. G. Wang, X. J. Li, Q. Yue, X. Dong, B. Du, W. Cao and Q. Wei, *Anal. Chem.*, 2019, **91**, 1989–1996.
6 A. Y. Chen, M. Zhao, Y. Zhuo, Y. Q. Chai and R. Yuan, *Anal. Chem.*, 2017, **89**, 9232–9238.
7 G. Valenti, E. Rampazzo, S. Bonacchi, L. Petrizza, M. Marcaccio, M. Montalti, L. Prodi and F. Paolucci, *J. Am. Chem. Soc.*, 2016, **138**, 15935–15942.
8 W. J. Miao, J. P. Choi and A. J. Bard, *J. Am. Chem. Soc.*, 2002, **124**, 14478–14485.
9 X. Q. Lv, M. Li, Z. H. Guo and X. W. Zheng, *Luminescence*, 2019, **34**, 334–340.
10 J. E. Dick, C. Renault, B. K. Kim and A. J. Bard, *J. Am. Chem. Soc.*, 2014, **136**, 13546–13549.
11 H. Z. Zheng and Y. B. Zu, *J. Phys. Chem. B*, 2005, **109**, 12049–12053.
12 Y. T. Zhang, B. S. Takale, F. Gallou, J. Reilly and B. H. Lipshutz, *Chem. Sci.*, 2019, **10**, 10556–10561.
13 W. Zhu, Z. Chen, Y. Pan, R. Y. Dai, Y. Wu, Z. B. Zhuang, D. S. Wang, Q. Peng, C. Chen and Y. D. Li, *Adv. Mater.*, 2018, 1800426.
14 X. N. Fang, Y. K. Duan, G. B. Adkins, S. Q. Pan, H. Wang, Y. Liu and W. W. Zhong, *Anal. Chem.*, 2018, **90**, 2787–2795.
15 A. Küchler, M. Yoshimoto, S. Luginbühl, F. Mavelli and P. Walde, *Nanotechnol*, 2016, **11**, 409–420.
16 Y. Y. Su, D. Wu, J. Chen, G. Chen, N. Hu, H. L. Wang, P. X. Wang, H. Y. Han, L. G. Li and Y. N. Wu, *Anal. Chem.*, 2019, **91**, 11687–11695.
17 H. Rothfuss, N. D. Knöfel, P. W. Roesky and C. Barner-Kowollik, *J. Am. Chem. Soc.*, 2018, **140**, 5875–5881.
18 H. Al-Kutubi, S. Voci, L. Rassaei, N. Sojic and K. Mathwig, *Chem. Sci.*, 2018, **9**, 8946–8950.
19 M. M. Richter, *Chem. Rev.*, 2004, **104**, 3003–3036.
20 L. L. Li, Y. Chen and J. J. Zhu, *Anal. Chem.*, 2017, **89**, 358–371.
21 M. Hesari, M. S. Workentin and Z. F. Ding, *Chem. Sci.*, 2014, **5**, 3814–3822.
22 J. M. Wang and B. Yan, *Anal. Chem.*, 2019, **91**, 13183–13190.
23 X. Feng, X. S. Ding and D. L. Jiang, *Chem. Soc. Rev.*, 2012, **41**, 6010–6022.
24 X. R. Wang, X. Han, J. Zhang, X. W. Wu, Y. Liu and Y. Cui, *J. Am. Chem. Soc.*, 2016, **138**, 12332–12335.
25 Y. F. Ma, F. Yuan, Y. Yu, Y. L. Zhou and X. X. Zhang, *Anal. Chem.*, 2020, **92**, 1424–1430.
26 C. R. DeBlase, K. E. Silberstein, T. T. Truong, H. D. Abruña and W. R. Dichtel, *J. Am. Chem. Soc.*, 2013, **135**, 16821–16824.
27 M. S. Lohse and T. Bein, *Adv. Funct. Mater.*, 2018, **28**, 1705553.
28 H. Li, J. H. Chang, S. S. Li, X. Y. Guan, D. D. Li, C. Y. Li, L. X. Tang, M. Xue, Y. S. Yan, V. Valtchev, S. L. Qiu and Q. R. Fang, *J. Am. Chem. Soc.*, 2019, **141**, 13324–13329.
29 Y. Z. Wang, S. Y. Ji, H. Y. Xu, W. Zhao, J. J. Xu and H. Y. Chen, *Anal. Chem.*, 2018, **90**, 3570–3575.
30 S. Y. Ding, J. Gao, Q. Wang, Y. Zhang, W. G. Song, C. Y. Su and W. Wang, *J. Am. Chem. Soc.*, 2011, **133**, 19816–19822.
31 X. Y. Niu, S. Y. Ding, W. F. Wang, Y. L. Xu, Y. Y. Xu, H. L. Chen and X. G. Chen, *J. Chromatogr. A*, 2016, **133**, 19816–19822.
32 R. Y. Lai and A. J. Bard, *J. Phys. Chem. A*, 2003, **107**, 3335–3340.